Available online at www.sciencedirect.com
SCIENCE DIRECT
Journal of Catalysis 241 (2006) 45–55
JOURNAL OF CATALYSIS
www.elsevier.com/locate/jcat

Effect of the support composition on the vapor-phase hydrogenation of crotonaldehyde over $Pt/Ce_xZr_{1-x}O_2$ catalysts

J.C. Serrano-Ruiz, J. Luettich, A. Sepúlveda-Escribano *, F. Rodríguez-Reinoso

Departamento de Química Inorgánica, Universidad de Alicante, Apartado 99, E-03080 Alicante, Spain

Received 13 December 2005; revised 17 February 2006; accepted 8 April 2006

Available online 22 May 2006

Abstract

Vapor-phase hydrogenation of toluene and selective hydrogenation of crotonaldehyde (2-butenal) have been performed at 333 K over Cl-free Pt/ZrO_2 and $Pt/Ce_xZr_{1-x}O_2$ catalysts ($0.2 \leqslant x \leqslant 0.8$) after reduction under H_2 at low (473 K) and high (773 K) temperatures. The catalysts were characterized by X-ray diffraction, Raman spectroscopy, temperature-programmed reduction, and X-ray photoelectron spectroscopy after each reduction treatment. An important effect of the support composition on the catalytic activity was observed for both reactions. The catalytic behavior of Pt in the two test reactions studied was strongly dependent on the support composition and on the reduction temperature. For toluene hydrogenation, after reduction at 473 K, catalytic activity was higher for catalysts with no or low ceria content. Furthermore, whereas the increase in the reduction temperature hardly modified the activity of Pt/ZrO_2, it strongly deactivated the catalysts with high cerium content in the support. For crotonaldehyde hydrogenation, on the other hand, increased reduction temperature produced a general increase in activity (except for the catalyst with the highest cerium content), along with an increase in selectivity toward the hydrogenation of the carbonyl bond to yield crotyl alcohol. The results are explained on the basis of the effect of partial reduction of Ce(IV) in the support.

Keywords: Pt catalysts; SMSI effect; Crotonaldehyde hydrogenation; Toluene hydrogenation; Ceria–zirconia mixed oxides

1. Introduction

Selective catalytic hydrogenation of organic substrates containing a number of unsaturated functional groups is an important step in the industrial preparation of fine chemicals and has been attracting much interest for fundamental research in catalysis. Allylic alcohols obtained by selective hydrogenation of the C=O group of α,β-unsaturated aldehydes are important intermediates for the production of perfumes, flavorings, and pharmaceuticals [1–3]. But hydrogenating a carbonyl bond in the presence of an olefinic bond [4] is not an easy task, due to the fact that the C=C bond is preferentially reduced by both thermodynamic and kinetic considerations. Monometallic platinum catalysts usually hydrogenate the C=C bond with 100% selectivity, and it is necessary to promote the metal to obtain a certain selectivity toward the hydrogenation of the carbonyl bond. This can be achieved by, among other methods, using a support that can interact with the metal after a reduction treatment, with TiO_2 [5,6], ZnO [7], and CeO_2 [8–10] the most commonly studied. Using this kind of support with strong metal–support interaction (SMSI) properties leads to an increase in activity and selectivity of noble metals in selective hydrogenation reactions involving unsaturated aldehydes like crotonaldehyde [6,8–11], cinnamaldehyde [12,13], furfural [14], and citral [15,16]. In all cases, the effect of the support seems to be related to activation of the C=O bond through the interaction of the oxygen atom with oxygen vacancies created at the metal–support interface on the reduction treatment.

On the other hand, it is well known that the incorporation of some elements, principally Zr, in the ceria lattice can change the redox and textural properties of the lattice. Thus, zirconium improves the reducibility of cerium by enhancing the mobility of oxygen through the CeO_2 lattice [17] and at the same time increases the thermal stability of CeO_2, thereby improving the metal–CeO_2 interaction. Cerium and zirconium are among the most widely studied and applied promoters in heterogeneous

* Corresponding author. Fax: +34 965 90 34 54.
E-mail address: asepul@ua.es (A. Sepúlveda-Escribano).

0021-9517/$ – see front matter
doi:10.1016/j.jcat.2006.04.006

catalytic reactions in recent years, due mainly to their important role in the three-way catalysts for the treatment of automobile exhaust gas [18–21]. However, cerium and zirconium oxides have been used very little for hydrogenation reactions. Relatively few works on CO hydrogenation by metals such as Pd, Rh, and Fe [22–25] and, more recently, on the vapor-phase hydrogenation of phenol [26] can be found in the literature.

This article reports the results of a study on the catalytic behavior of platinum catalysts supported on cerium–zirconium mixed oxides with different Ce/Zr ratios in the vapor-phase hydrogenation of crotonaldehyde. The study focused on the effect of the reduction temperature and the support composition on the catalytic properties of platinum. Results obtained in the vapor-phase hydrogenation of toluene (a structure-insensitive reaction) are also included for the sake of comparison.

2. Experimental

The supports, ceria–zirconia mixed oxides with various molar compositions, were prepared from nitrate precursors by a precipitation method. Aqueous solutions of $Ce(NO_3)_3 \cdot 6H_2O$ (Aldrich, 99%) and $ZrO(NO_3)_2$ (Fluka, 98%) were used with the appropriate concentration to obtain the desired Ce/Zr ratio. Once the solutions were mixed, concentrated aqueous NH_3 was slowly added to maintain a pH of 10 during the precipitation process. Finally, the resulting slurry was stirred at room temperature for 65 h. The solids were separated by filtration, washed with ultra-pure water and ethanol, dried at 383 K overnight, and calcined in air at 723 K for 2 h, with a heating rate of 3 K min^{-1}. These are referred to as $Ce_xZr_{1-x}O_2$ ($0.2 \leqslant x \geqslant 0.8$) hereinafter. Pure zirconium dioxide was prepared in a similar way, but with calcination conditions of 773 K for 15 h [27]. The actual bulk CeO_2 and ZrO_2 content of the supports was determined by X-ray fluorescence, as reported in Table 1.

Catalysts were prepared by impregnating the supports with aqueous solutions of $[Pt(NH_3)_4](NO_3)_2$ (Aldrich, 99%). Excess solution was removed by gentle evaporation under flowing nitrogen at 308 K. Finally, the catalysts were dried overnight at 383 K and calcined in air at 673 K for 2 h. The catalysts' platinum content was determined by ultraviolet analysis of the solutions obtained after the samples were dissolved in aqua regia at 313 K; these values are reported in Table 2.

The surface area of the supports was determined on a Coulter Omnisorp 610 by N_2 adsorption at 77 K; the results were analyzed by the BET method. Before measurements, the samples were dried at 383 K for 12 h and outgassed at 523 K under vacuum.

X-Ray powder diffraction (XRD) patterns were recorded on a JSO Debye-flex 2002 system (Seifert), fitted with a Cu cathode and a Ni filter, using a 2° min^{-1} scanning rate. Raman spectra were recorded on a 50-mW LabRam spectrometer (Yobin–Yvon Horiba) equipped with an Ar laser (514.5 nm) as the excitation source. Detection was done with a CCD (1064 × 256 pixels) refrigerated with a Peltier system.

Temperature-programmed reduction (TPR) measurements were carried out in a U-shaped quartz cell using a 5% H_2/He gas flow of 50 cm^3 min^{-1} and about 0.15 g of sample, with a heating rate of 10 K min^{-1}. The sample was treated with flowing He at 313 K for 1 h before the TPR run. Hydrogen consumption was followed by on-line mass spectrometry.

X-Ray photoelectron spectroscopy (XPS) was performed with a VG-Microtech Multilab 3000 spectrometer equipped with a hemispherical electron analyzer and a Mg-K_α (h = 1253.65 eV; 1 eV = 1.6302×10^{-19} J) 300-W X-ray source. The powder samples were pressed into small Inox cylinders, mounted on a sample rod placed in a pretreatment chamber, and reduced in flowing H_2 for 1 h at 473 and 773 K before being transferred to the analysis chamber. Before the spectra were recorded, the sample was maintained in the analysis chamber until a residual pressure of ca. 5×10^{-7} N m^2 was reached. The spectra were collected at a pass energy of 50 eV. The intensities were estimated by calculating the integral of each peak after subtracting the S-shaped background, then fitting the experimental curve to a combination of Lorentzian (30%) and Gaussian (70%) lines. All binding energies were referenced to the C 1s line at 284.6 eV, which provided binding energy values with a accuracy of ±0.2 eV. The surface Pt/(Ce + Zr) atomic ratios were estimated from the integrated intensities corrected by the atomic sensitivity factors [28].

The catalytic behavior of the samples in the vapor-phase hydrogenation of crotonaldehyde (2-butenal [CROALD]) was tested in a microflow reactor at atmospheric pressure under differential conditions. Before their catalytic behaviors were evaluated, the catalysts (around 0.15 g) were reduced in situ at 473 and 773 K under flowing hydrogen (50 cm^3 min^{-1}) for 10 h, then cooled under hydrogen to the reaction temperature (333 K). Then, the catalysts were contacted with a reaction mixture (total flow, 50 cm^3 min^{-1}; H_2/CROALD ratio, 26) containing purified hydrogen and crotonaldehyde (Fluka, >99.5%) prepared by passing a hydrogen flow through a thermostabilized saturator (at 293 K) containing the unsaturated aldehyde. These conditions led to a reciprocal space time $W/F_{\mathrm{Crot},0}$ of 30.5 g_{cat} h mol^{-1}, where W is the weight of catalyst and $F_{\mathrm{Crot},0}$ is the molar feed flow of crotonaldehyde. The selectivity to

Table 1
Bulk composition and BET surface areas of supports

Support	Bulk CeO_2 content (%)	Bulk ZrO_2 content (%)	Surface BET (m^2/g)
$Ce_{0.8}Zr_{0.2}O_2$	76	24	99
$Ce_{0.68}Zr_{0.32}O_2$	65	35	100
$Ce_{0.5}Zr_{0.5}O_2$	45	55	115
$Ce_{0.20}Zr_{0.8}O_2$	16	84	52
ZrO_2	0	100	65

Table 2
Pt loading in catalysts (wt%)

Catalysts Pt/$Ce_xZr_{1-x}O_2$	Pt loading (wt%)
Pt/$Ce_{0.8}Zr_{0.2}O_2$	1.98
Pt/$Ce_{0.68}Zr_{0.32}O_2$	1.62
Pt/$Ce_{0.5}Zr_{0.5}O_2$	1.88
Pt/$Ce_{0.20}Zr_{0.8}O_2$	0.75
Pt/ZrO_2	1.48

the desired product i was calculated as $S_i = (\text{moles of product } i / \sum \text{moles of products}) \times 100$. Toluene hydrogenation was studied at 333 K, with a reactant mixture containing purified toluene (Aldrich, HPLC grade) at a H_2/C_7H_8 ratio of 36, with a $W/F_{\text{Tol},0}$ of 42.5 $g_{cat}\,h\,mol^{-1}$. The concentrations of the reactants and the products at the reactor outlet were determined by on-line gas chromatography with a Carbowax 20 M 58/90 semicapillary column.

3. Results and discussion

3.1. Textural and structural characterization

Table 1 reports the relative CeO_2 and ZrO_2 content in the supports, as determined by X-ray fluorescence spectroscopy. The oxide compositions cover a wide range, from pure zirconia to 76 mol% CeO_2. Hereinafter, samples are labelled with the nominal composition, which in all cases differs only slightly from the actual one.

The N_2 BET surface areas of the different supports are also reported in Table 1. Surface areas of around 100 $m^2\,g^{-1}$ are obtained for the supports with higher cerium content ($x \geqslant 0.5$), whereas pure zirconia and $Ce_{0.2}Zr_{0.8}O_2$ have surface areas of only 65 and 52 $m^2\,g^{-1}$, respectively. These data are related to the structural properties of the supports, as discussed below.

The XRD patterns for the $Ce_xZr_{1-x}O_2$ supports calcined at 723 K and pure ZrO_2 calcined at 773 K are shown in Fig. 1. For the pure zirconia support, the pattern can be assigned to a mixture of monoclinic and tetragonal phases. The cerium-containing supports show a transition from a pure cubic phase for the high Ce content ($x > 0.5$) materials to the presence of a tetragonal phase together with the cubic one, in supports with lower cerium content ($x \leqslant 0.5$). This is in agreement with the results obtained by Yashima et al. [29]. The shift of the ceria-phase diffraction peaks toward higher 2θ values can be interpreted as resulting from a mixed oxide in which the substitution of the Ce^{4+} by the smaller Zr^{4+} ions produces changes in the lattice parameters [30–34]. Broad diffraction peaks were detected in all cases, indicating the presence of small oxide particles.

XRD patterns corresponding to the calcined catalysts (at 673 K; not shown) are similar to those obtained with the supports. No peaks corresponding to platinum phases can be observed, indicating the presence of very small metal particles in all cases.

Raman spectra of the mixed oxide supports are collected in Fig. 2. The spectra obtained with the Ce rich oxides are dominated by a strong band at around 470 cm^{-1}, which is assigned to the F_{2g} Raman active mode of a material with fluorite-type structure. A weak shoulder can also be observed near 600 cm^{-1} due to the LO mode of CeO_2, which appears because of the relaxation of symmetry rules [35]. The intensity of the band at 470 cm^{-1} diminishes as the cerium content decreases, in such a way that it nearly disappears in $Ce_{0.2}Zr_{0.8}O_2$. For this sample, new bands appear at 254, 316, and 613 cm^{-1}, characteristic of a tetragonal structure. These findings corroborate those obtained by XRD diffraction: the existence of a cubic fluorite-type structure for high-cerium content supports ($x > 0.5$), with the appearance of a tetragonal phase as the cerium content decreases for oxides with $x \leqslant 0.5$.

3.2. Temperature-programmed reduction

The reduction properties of the mixed oxides used as supports were studied by TPR; the hydrogen consumption profiles obtained as a function of temperature are plotted in Fig. 3. The TPR profile of pure CeO_2 (not shown here) is characterized by two peaks. The peak at the lower temperature (about 800 K) is assigned to the reduction of the more superficial Ce^{4+} and thus is very sensitive to the surface area of the oxide. The second peak, appearing at about 1100 K, originates from the bulk reduction of the oxide [36]. TPR profiles of mixed oxides in Fig. 3 show a main reduction peak centered at about 850 K; only the sample with the highest cerium content ($Ce_{0.8}Zr_{0.2}O_2$) shows a small broad peak at a higher temperature. The easier reduction of the CeO_2–ZrO_2 mixed oxides compared with pure CeO_2 has been reported by several authors [34,37]. It is due to the structural modifications induced in the cubic fluorite-type structure of ceria when some Ce^{4+} cations are substituted with

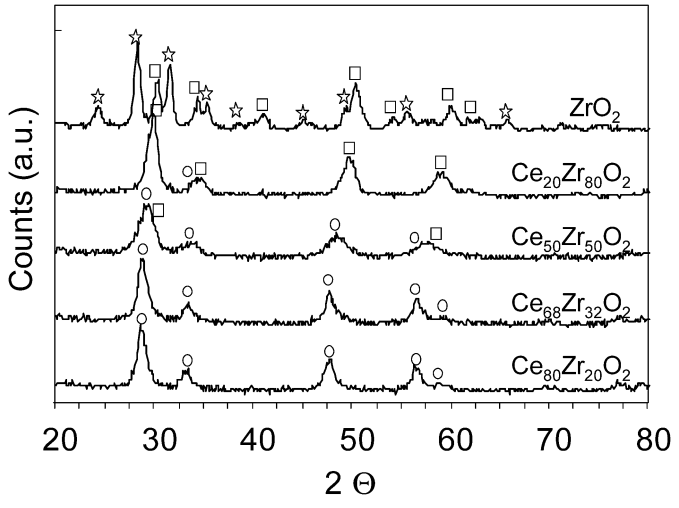

Fig. 1. XRD patterns of $Ce_xZr_{1-x}O_2$ supports (circles, cubic phase; square, tetragonal phase; star, monoclinic phase).

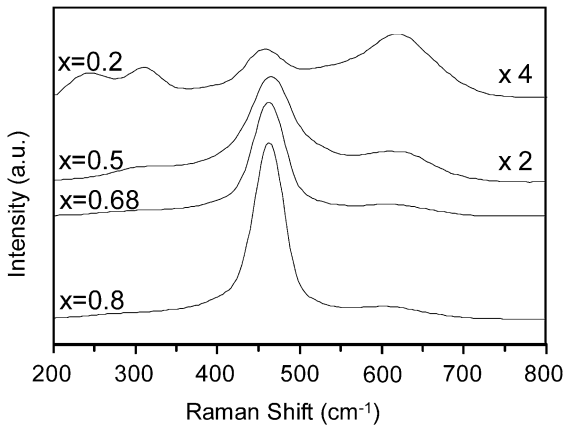

Fig. 2. Raman spectra of $Ce_xZr_{1-x}O_2$ supports.

smaller Zr^{4+} cations, thereby favoring the diffusion of O^{2-} anions within the lattice. Thus, the TPR profiles in Fig. 3 are indicative of the mixed-oxide character of the supports.

Fig. 3 also shows that the reduction peaks shift to higher temperatures as the cerium content decreases. This findings has been reported previously [38] and seems to be related to increased oxygen mobility favored by the higher concentration of Ce^{4+} ions that can be reduced [39]. These data are in good agreement with several works [20,40,41] proposing that the presence of an irreducible structure like ZrO_2 in the mixed oxide is responsible for the shift observed for the maximum. The TPR profile for ZrO_2 shows no hydrogen consumption, as expected.

Different TPR profiles are obtained for the $Pt/Ce_xZr_{1-x}O_2$ catalysts (Fig. 4). Pt/ZrO_2 shows no reduction peaks, whereas cerium-containing catalysts give rise to at least two peaks. The low reduction temperature peak (around 450–500 K) is commonly assigned to the reduction of ceria in close contact with the metal, as well as to the reduction of platinum (breakdown of Pt–O–CeO_2 species created on calcination). The second peak, at about 650–700 K, is related to the surface reduction of CeO_2 not in close contact with the platinum. It should be noted that the presence of platinum clearly promotes the reduction of surface ceria, as evidenced by the shift of the peak at around

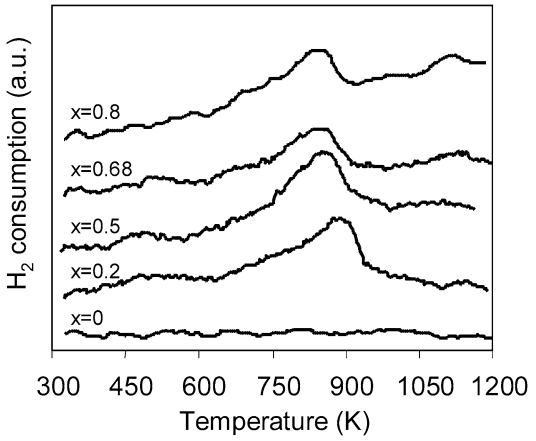

Fig. 3. Temperature-programmed reduction profiles of supports.

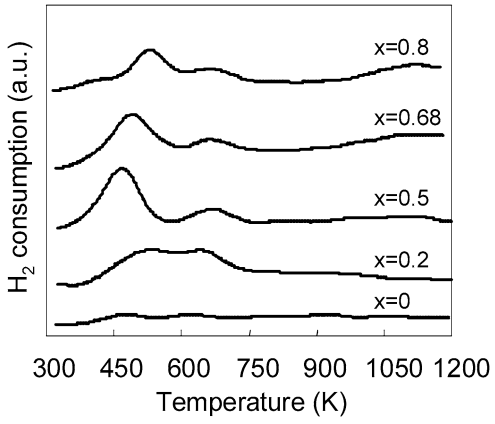

Fig. 4. Temperature-programmed reduction profiles of $Pt/Ce_xZr_{1-x}O_2$ catalysts.

800–900 K (in supports) to below 700 K (in catalysts). This phenomenon is assigned to the ability of the noble metal to promote the reduction of CeO_2 via spilling of hydrogen species over the support. In any case, there are clear differences among the different catalysts, with the easiest reduction obtained for $Pt/Ce_{0.5}Zr_{0.5}O_2$, for which the main reduction peak appears at only 450 K.

In conclusion, it seems clear from these results that in all cerium-containing catalysts, the reduction treatment at 773 K is sufficient to produce the surface reduction of ceria, with the creation of oxygen vacancies and the presence of Ce^{3+} ions. On the other hand, reduction at 473 K should affect the catalysts to a different extent, with the greatest reduction obtained for catalyst $Pt/Ce_{0.5}Zr_{0.5}O_2$.

3.3. X-Ray photoelectron spectroscopy

The surface composition of the $Pt/Ce_xZr_{1-x}O_2$ catalysts was analyzed by XPS after calcination at 673 K. The most interesting results are summarized in Table 3. It can be seen that the Zr $3d_{5/2}$ binding energy remains unchanged, within the precision limits of the measurement, at around 182.2 eV (typical binding energy for Zr^{4+}) for the entire range of compositions. However, there seems to be a shift of the positions of the O 1s band. The higher the cerium content, the lower the O 1s binding energy. This result can be explained in terms of the structural properties of the supports. XRD and Raman spectroscopy have shown that $Pt/Ce_xZr_{1-x}O_2$ catalysts with $x \geqslant 0.5$ have a cubic structure, in which Zr^{4+} is incorporated into the CeO_2 lattice. It has been found that Ce^{4+} is reduced at lower temperatures when it is incorporated into cubic structures rather than into tetragonal structures. In addition, it is well known that cubic symmetry favors oxygen diffusion through the lattice due to an adequate size of the channels for oxygen migration [30,31,33,34], and a decrease in the binding energy of oxygen would be expected as the cerium content increases.

With regard to the Ce/Zr atomic ratio, it should be noted that the $(Ce/Zr)_{bulk}$ ratio (obtained by X-ray fluorescence measurements) is close to $(Ce/Zr)_{XPS}$ in all cases except $Pt/Ce_{0.8}Zr_{0.2}O_2$. This means that there is no surface segregation, with the surface composition of the solid solutions being similar to that of the bulk. In $Pt/Ce_{0.8}Zr_{0.2}O_2$, the Ce/Zr ratio in the bulk is higher than in the surface, indicating surface enrichment in zirconium. This partial segregation was not detected by XRD and can be described as a migration of Zr^{4+} cations toward the periphery of the particles, whereas the Ce^{4+}

Table 3
XPS characterization of $Pt/Ce_xZr_{1-x}O_2$ catalysts

Catalyst	O 1s BE (eV)	Zr $3d_{5/2}$ BE (eV)	$(Ce/Zr)_{bulk}$[a]	$(Ce/Zr)_{XPS}$
$Pt/Ce_{0.8}Zr_{0.2}O_2$	529.8	182.2	3.17	2.45
$Pt/Ce_{0.68}Zr_{0.32}O_2$	529.9	182.2	1.86	1.71
$Pt/Ce_{0.5}Zr_{0.5}O_2$	530.0	182.2	0.82	0.77
$Pt/Ce_{0.20}Zr_{0.8}O_2$	530.1	182.2	0.19	0.17
Pt/ZrO_2	530.3	182.0	–	–

[a] Results obtained from XRF measurements.

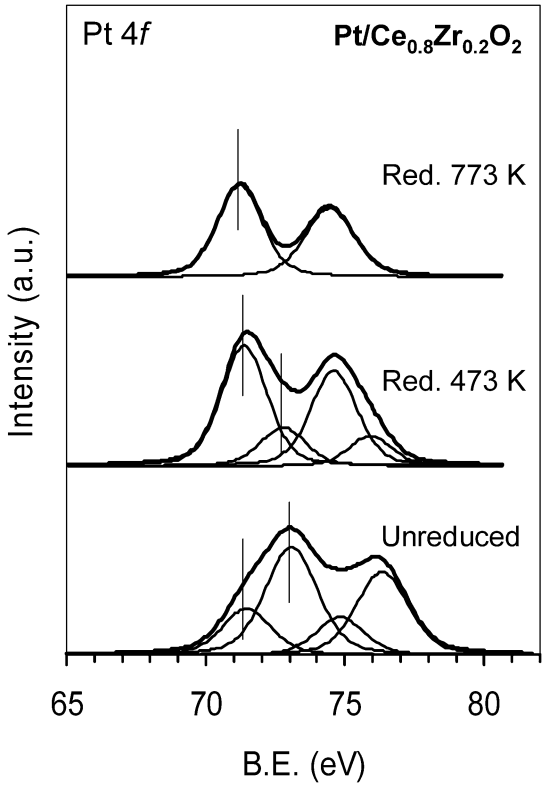

Fig. 5. XPS Pt 4f spectra of calcined and reduced $Pt/Ce_{0.8}Zr_{0.2}O_2$ catalysts.

concentration increases in the center. Bozo et al. [20] proposed a "cherry" model to explain this result, with a core composed mainly of a cubic Ce-rich phase and an outer part richer in a tetragonal Zr-rich phase.

The effect of the reduction temperature on the surface composition of the catalysts was also studied by XPS. The catalysts were reduced in situ with H_2 at 473 and 773 K before the measurements were obtained. Fig. 5 shows the Pt 4f spectra for the uncalcined and reduced samples are shown as a representative sample for $Pt/Ce_{0.8}Zr_{0.2}O_2$. Two broad bands appear, corresponding to the Pt $4f_{7/2}$ (at lower binding energies) and Pt $4f_{5/2}$ levels (at higher binding energies). The XPS spectra indicate a shift of the Pt 4f binding energies toward lower values as the reduction temperature is increased. The Pt 4f band is deconvoluted in two components corresponding to Pt(II) (around 73.0 eV) and Pt^0 (around 71.0 eV) species. The presence of a certain amount of reduced Pt should be noted even in the just-calcined catalysts. On the other hand, complete reduction of platinum is achieved only after reduction at high temperature (773 K), with samples reduced at 473 K containing a certain amount of oxidized platinum depending on the support. Fig. 6 plots the amount of metallic platinum (%) as a function of the cerium content in the support after the various reduction treatments. As mentioned before, a given amount of metallic platinum is already obtained after calcination in all samples except $Pt/Ce_{0.5}Zr_{0.5}O_2$. Thus, for the low-ceria content supports, nearly 50% of the platinum is already reduced after calcination, and for supports with $x \geqslant 0.5$, the amount of reduced platinum increases from 0 (for $x = 0.5$) to 28.5% (for $x = 0.8$). For the reduced catalysts, it is interesting to observe that only catalysts

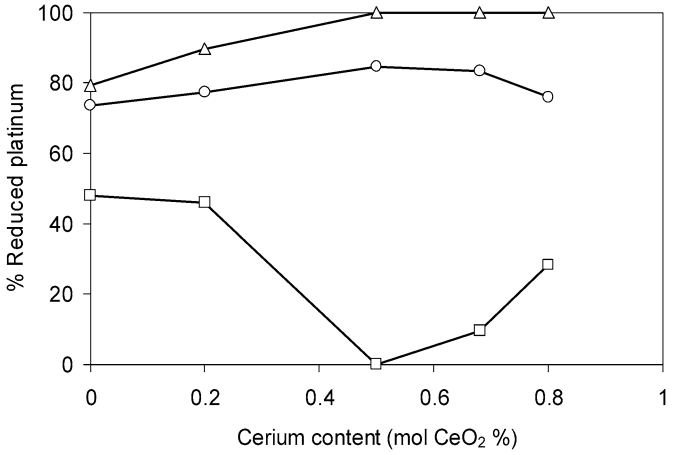

Fig. 6. Relative amount of metallic Pt in $Pt/Ce_xZr_{1-x}O_2$ catalysts, after different reduction treatments, as a function of the cerium content (□, unreduced; ○, reduced at 473 K; △, reduced at 773 K).

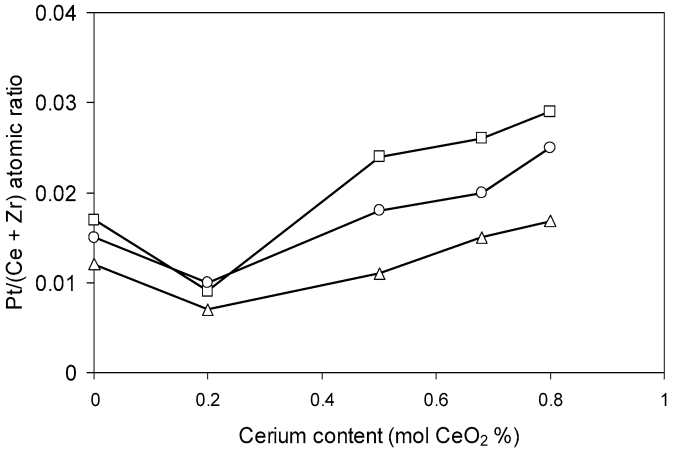

Fig. 7. Atomic Pt/(Ce + Zr) XPS ratios in $Pt/Ce_xZr_{1-x}O_2$ catalysts, as a function of the cerium content, after different reduction treatments (□, unreduced; ○, reduced at 473 K; △, reduced at 773 K).

with high cerium content ($x \geqslant 0.5$) showed a total reduction of platinum after treatment at 773 K. Furthermore, the difference between the amount of metallic platinum after reduction at low (473 K) and high (773 K) temperatures also increases with the amount of cerium in the support, with the greatest difference seen in $Pt/Ce_{0.8}Zr_{0.2}O_2$.

Fig. 7 plots the atomic Pt/(Ce + Zr) XPS ratios, which can be considered a measure of platinum dispersion in the catalysts, as a function of the cerium content in the supports, after the different reduction treatments. In general, the Pt/(Ce + Zr) ratios decrease as the reduction temperature increases, although two different behaviors can be can be envisaged. For catalysts with $x \leqslant 0.2$ supports, very little modification in the Pt/(Ce + Zr) ratios is observed between the calcined samples and those reduced at 473 K; the effect is somewhat larger after reduction at 773 K. In any case, platinum dispersion, measured as Pt/(Ce + Zr) ratio, decreases with the cerium content in the support. On the other hand, for catalysts with larger amounts of cerium in the support ($x \geqslant 0.5$), reduction at 473 K already produces a large decrease in Pt dispersion as measured

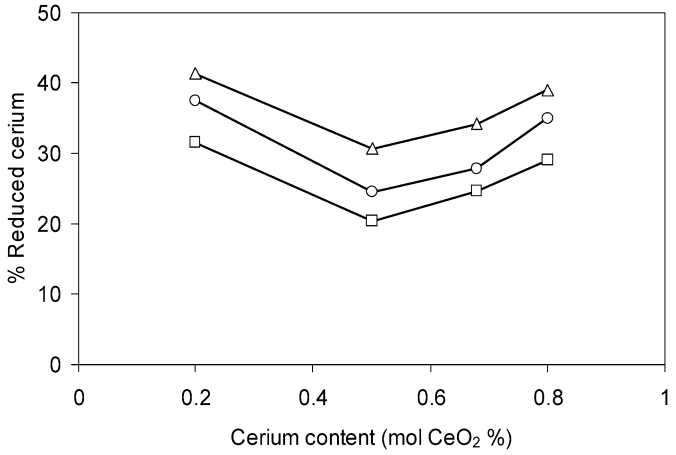

Fig. 8. Relative amount of surface Ce(III) (%) in Pt/$Ce_xZr_{1-x}O_2$ catalysts, as a function of the cerium content, after different reduction treatments (□, unreduced; ○, reduced at 473 K; △, reduced at 773 K).

by XPS, with a similar decrease after reduction at 773 K. It is also significant that platinum dispersion after a given treatment (as measured by XPS) increases with the cerium content in the support, which can be related to the well-known ability of CeO_2 to promote metal dispersion in ceria-supported noble metal catalysts [42].

The chemical state of cerium ions in the catalysts after the different reduction treatments was also studied by XPS. The analysis of the Ce 3d XP spectra is not easy, due to its complexity, which arises from the hybridization between the Ce 4f levels and the O 2p states [43]. The two sets of spin-orbital multiplets, corresponding to the $3d_{3/2}$ and $3d_{5/2}$ contributions, are labeled u and v, respectively. Up to five peaks for each contribution can be obtained by a curve-fitting analysis [44,45]. Different approaches have been used to evaluate the degree of ceria reduction from the XPS spectra; possibly the most commonly used approach considers the contribution of peaks that are representative of Ce^{3+} to the total Ce 3d region [9,44,46]. The relative amounts of Ce^{3+} in the catalysts after the various reduction treatments are plotted in Fig. 8 as functions of the bulk cerium content. It can be seen that in all cases, there is a certain amount of Ce^{3+} even in the unreduced catalysts, which is assigned to the partial reduction of Ce^{4+} ions during the XPS experiments [46,47]. One parameter that mainly affects the photoreduction of CeO_2 during XPS analysis is its crystallinity, in such a way that amorphous cerium oxide samples are reduced more extensively than crystalline materials [48]. Taking into account that the supports have been prepared in a similar way, and that the XRD patterns indicate a close degree of crystallinity, it can be assumed that the reducibility of Ce^{4+} in the catalysts, both after calcination and after the reduction treatments, is due mainly to their own composition. As expected, the relative amount of Ce^{3+} increases with the reduction temperature, but as shown in Fig. 8, there is a similar trend after the various treatments. The relative amount of Ce^{3+} is the highest in $Ce_{0.2}Zr_{0.8}O_2$, passes through a minimum for $Ce_{0.5}Zr_{0.5}O_2$, and then increases with increasing cerium content. However, taking into account that a significant amount of Ce^{4+} in the calcined (unreduced) catalysts is already reduced, and that the XPS spectra are obtained successively on the same sample, a more adequate estimation of the degree of reduction of the support would be obtained by considering the results on the unreduced samples as a baseline. In this way, the relative amount of Ce^{3+} after reduction at 773 K would be similar in all catalysts, around 10% higher than that obtained in the unreduced samples. On the other hand, appreciable differences can be observed after reduction at 473 K. In this case, the degree of reduction would be higher in $Pt/Ce_{0.2}Zr_{0.8}O_2$ and $Pt/Ce_{0.8}Zr_{0.2}O_2$ (around 6% higher than in the unreduced samples) and lower in catalysts with intermediate cerium content.

3.4. Catalytic behavior

3.4.1. Toluene hydrogenation

It is generally acknowledged that assessing the metallic dispersion in supported metal catalysts containing ceria [49] is not an easy task. There are several reasons for this. First, ceria per se can chemisorb most probe molecules used in chemisorption techniques for metallic dispersion evaluation, such as H_2 and CO. Second, it is known that in the presence of highly dispersed metals at room temperature, large amounts of hydrogen can be transferred from the metal to the ceria support (spillover), falsifying the metallic dispersion results. On the other hand, the poor contrast between cerium and metals such as platinum makes it difficult to detect highly dispersed metal particles in transmission electron microscopy images. In this way, alternative specific procedures, such as low-temperature hydrogen chemisorption [50], quantitative measurements of the ν_{CO} band intensity [51], and measurement of the catalytic activity in a structure-insensitive reaction, have been used to estimate the metallic dispersion in this kind of system. In the latter case, the catalytic activity in the structure-insensitive reaction would depend only on the number of metal atoms available at the surface of the catalysts and would not be affected by the metal particle size or the crystallographic plane. Thus, benzene [8] and toluene [6,9] hydrogenation, as well as cyclohexane dehydrogenation [52], have been used to successfully estimate the fraction of metal exposed in noble metal catalysts promoted by ceria. However, it must be kept in mind that the structure-insensitive character of these reactions may be affected by any electronic and/or geometrical effect due to partially reduced ceria on the metal particles that could be generated on reduction at high temperature. To avoid this problem, we use the measurements of catalytic activity in a structure-insensitive reaction, such as toluene hydrogenation, only as a reference to analyze the effect of reduction treatments on the catalysts. We then compare these results with those obtained in a very different reaction, such as crotonaldehyde hydrogenation.

Table 4 reports the catalytic activity (after 120 min on stream) for toluene hydrogenation ($\mu mol\ s^{-1}\ g_{Pt}^{-1}$) at 333 K after reduction at 473 and 773 K, as well as the decrease in activity (%) at high reduction temperature. The increased cerium content in the support produces a significant decrease in catalytic activity after reduction at both 473 and 773 K. Table 4 shows that for catalysts reduced at 473 K, there is a decrease

Table 4
Catalytic activity ($\mu mol\, s^{-1}\, g_{Pt}^{-1}$) in toluene hydrogenation at 333 K, and decrease (%) after reduction at high temperature (773 K)

	Pt/ZrO_2	$Pt/Ce_{0.20}Zr_{0.8}O_2$	$Pt/Ce_{0.5}Zr_{0.5}O_2$	$Pt/Ce_{0.68}Zr_{0.32}O_2$	$Pt/Ce_{0.8}Zr_{0.2}O_2$
Reduction temperature (K)					
473	95.0	69.5	27.0	22.8	20.8
773	92.5	46.5	10.8	2.4	0.8
Decrease (%)	3	33	60	89	96

in activity (per amount of Pt in the catalyst) from Pt/ZrO_2 to $Pt/Ce_{0.2}Zr_{0.8}O_2$, which can be correlated with the decrease in the amount of surface platinum detected by XPS (Fig. 7). When the amount of cerium in the support increases ($x \geqslant 0.5$), the catalytic activity in toluene hydrogenation strongly decreases compared with that in Pt/ZrO_2, with activity being rather similar for the three catalysts despite the fact that the amount of surface platinum detected by XPS increases. The strong metal–support interaction effect due to the partially reduced support is not expected after reduction at low temperature. In this way, and taking into account the structure-insensitive character of toluene hydrogenation, these activity values should be related to a decrease in the number of surface platinum sites available for the reaction. However, it must be kept in mind that the catalytic activity may be affected by other properties of the support besides reducibility. Lin and Vannice [53] showed that the rate of toluene hydrogenation on platinum catalysts was enhanced by the support acidity. For platinum supported on SiO_2, η-Al_2O_3, $SiO_2 \cdot Al_2O_3$, and TiO_2, these authors observed that the activation energies for toluene hydrogenation, as well as the reaction orders, had no dependence on the support, but the turnover frequencies were four times higher for the most acidic support ($Pt/SiO_2 \cdot Al_2O_3$) compared with the least acidic support (SiO_2). This rate enhancement was attributed to an additional hydrogenation reaction occurring via hydrogen spilling over the support surface and reacting with toluene adsorbed on acid sites on the oxide.

After reduction at 773 K, Pt/ZrO_2 hardly loses activity with respect to that obtained after reduction at 473 K. However, deactivation becomes more and more important as the amount of cerium in the support increases. The results shown in Fig. 7 indicate that the amount of surface platinum as detected by XPS decreases after reduction at 773 K, but the trend in relation to the cerium content of the support is similar to that obtained after reduction at 473 K. Thus, the strong catalyst deactivation after reduction at 773 K, which becomes more significant as the amount of cerium in the support increases, is not due to a loss of surface platinum but rather must be assigned to the strong metal–support interaction effect induced after reduction at high temperature [8]. This effect is related to the presence of partially reduced ceria and has been explained based on two mechanisms: (1) geometrical effects, such as the formation of intermetallic Pt–Ce compounds [54] and the coverage of platinum particles by ceria patches [55], and (2) electronic effects arising from the electronic transfer between the platinum particles and partially reduced ceria. The modification of the electron density in platinum would affect the strength of the platinum–benzene bond, hindering benzene hydrogenation. The latter mechanism seems more likely in this case, because the reduction temperature is too low to produce metallic cerium and the migration of partially reduced ceria patches has not been observed for reduction temperatures below 973 K [56].

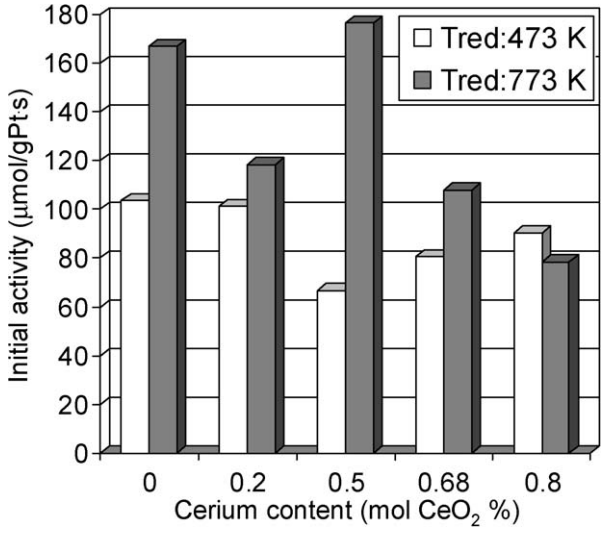

Fig. 9. Initial catalytic activity for crotonaldehyde hydrogenation for $Pt/Ce_xZr_{1-x}O_2$ catalysts at 333 K, after reduction at 473 and 773 K.

3.4.2. Crotonaldehyde hydrogenation

Here we discuss the effect of the cerium content in the supports on the catalytic behavior of the samples in a reaction such as crotonaldehyde hydrogenation. During the first stages of the reaction, carbon balance is not achieved, mainly due to the adsorption of reactant and products on the support. Once the balance is obtained (i.e., when the amount of crotonaldehyde leaving the reactor is equal to that fed minus that transformed into products), reaction rates are measured. Fig. 9 shows the initial overall activity (after 5 min on stream) of catalysts in the vapor-phase hydrogenation of crotonaldehyde at 333 K, after reduction treatments at both 473 and 773 K. It can be seen that after reduction at 473 K, catalysts with low cerium content ($x < 0.5$) exhibit higher initial activities than those with high cerium content. After reduction at 773 K, an increase of initial activity values is seen for all catalysts studied except $Pt/Ce_{0.8}Zr_{0.2}O_2$, which shows a slight decrease in activity after reduction at high temperature. After the first stages of reaction, activity strongly drops in all cases. This deactivation of the catalysts has been related to the decarbonylation of the reactant molecule yielding carbon monoxide, which is irreversibly adsorbed on platinum at the reaction conditions [57]. Figs. 10 and 11 show the evolution of catalytic activity for all catalysts versus time on

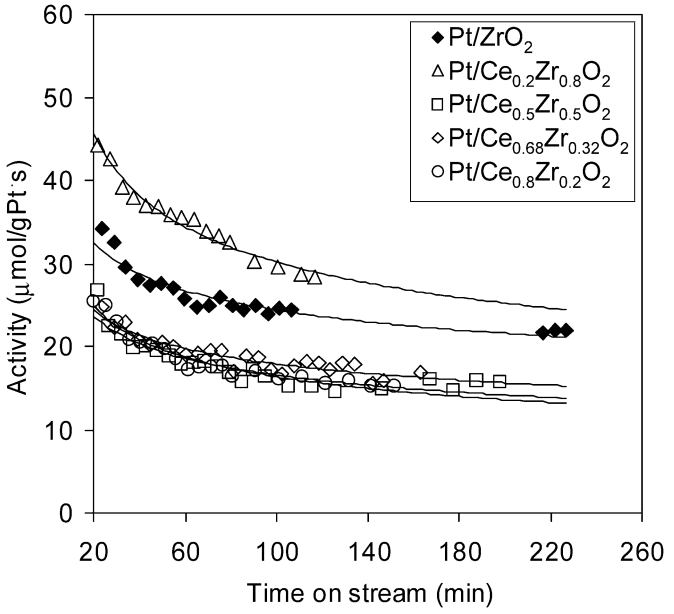

Fig. 10. Catalytic activity for crotonaldehyde hydrogenation for catalysts $Pt/Ce_xZr_{1-x}O_2$ as a function of time on stream at 333 K, after reduction at 473 K.

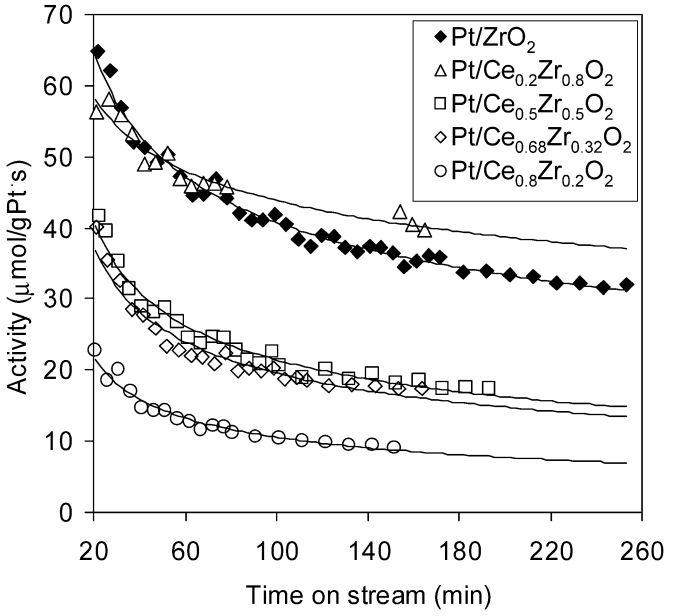

Fig. 11. Catalytic activity for crotonaldehyde hydrogenation for catalysts $Pt/Ce_xZr_{1-x}O_2$ as a function of time on stream at 333 K, after reduction at 773 K.

stream obtained after reduction at 473 and 773 K, respectively. Fig. 10 shows that after reduction at 473 K, steady-state catalytic activity follows the order $Pt/Ce_{0.20}Zr_{0.8}O_2 > Pt/ZrO_2 > Pt/Ce_{0.5}Zr_{0.5}O_2 \approx Pt/Ce_{0.68}Zr_{0.32}O_2 \approx Pt/Ce_{0.8}Zr_{0.2}O_2$. This trend is different than that seen for toluene hydrogenation, in which the most active catalyst is Pt/ZrO_2. After reduction at 773 K (Fig. 11), activity evolution shows a different trend; catalysts with low cerium content ($x < 0.5$) have similar activity, whereas catalysts with high cerium content ($x \geqslant 0.5$) are less active as cerium content increases.

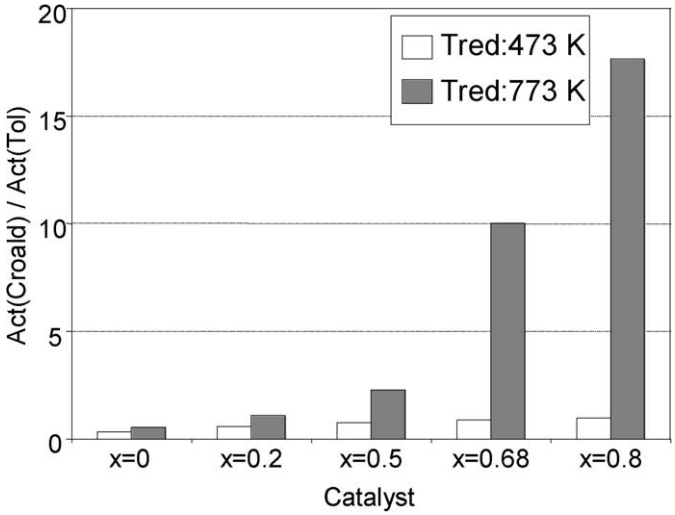

Fig. 12. Activity ratios for crotonaldehyde hydrogenation and toluene hydrogenation for catalysts reduced at 473 and 773 K.

Data for toluene hydrogenation show that a more drastic reduction treatment (from 473 to 773 K) leads to a strong decrease in catalytic activity, related to a strong metal–support interaction effect (Table 4). But this effect does not negatively affect the activity in crotonaldehyde hydrogenation. Fig. 12 plots the activity ratios between crotonaldehyde hydrogenation and toluene hydrogenation after the different reduction treatments. Although the ratio increases with the cerium content in the support after reduction at low temperature (473 K), this increase is much more significant after reduction at 773 K. Thus, whereas Pt/ZrO_2 shows a similar activity for both reactions, $Pt/Ce_{0.8}Zr_{0.2}O_2$ is 17 times more active for crotonaldehyde hydrogenation than for toluene hydrogenation.

Although results for catalytic activity cannot be explained straightforwardly because of the conjunction of several factors (mainly the intrinsic activity of the catalyst and the more or less pronounced deactivation), one other interesting indicator of the support effect in this system is the evolution of selectivity. The products obtained under the conditions used in this study are butanal (formed by hydrogenation of the C=C bond), crotyl alcohol (but-2-en-ol, formed by hydrogenation of the carbonyl C=O bond), butanol (formed on hydrogenation of the primary products butyraldehyde and crotyl alcohol), and the light hydrocarbons butane (formed through butanol hydrogenation) and propane, which result from decarbonylation reactions. Fig. 13 plots the selectivity to crotyl alcohol (molar fraction %) as a function of time on stream after reduction at 473 and 773 K. Table 5 reports the corresponding conversion values. After reduction at 473 K, Pt/ZrO_2 shows higher selectivity values than the cerium-containing catalysts during all stages of reaction, yielding a maximum value of 18 mol% selectivity at the initial reaction stages. Reduction at 773 K produces a strong increase in the selectivity to crotyl alcohol for all catalysts studied. Furthermore, higher cerium content in the support leads to a higher value of selectivity during the initial stages of reaction (reaction time, 5 min), with a maximum value of 66 mol% selectivity.

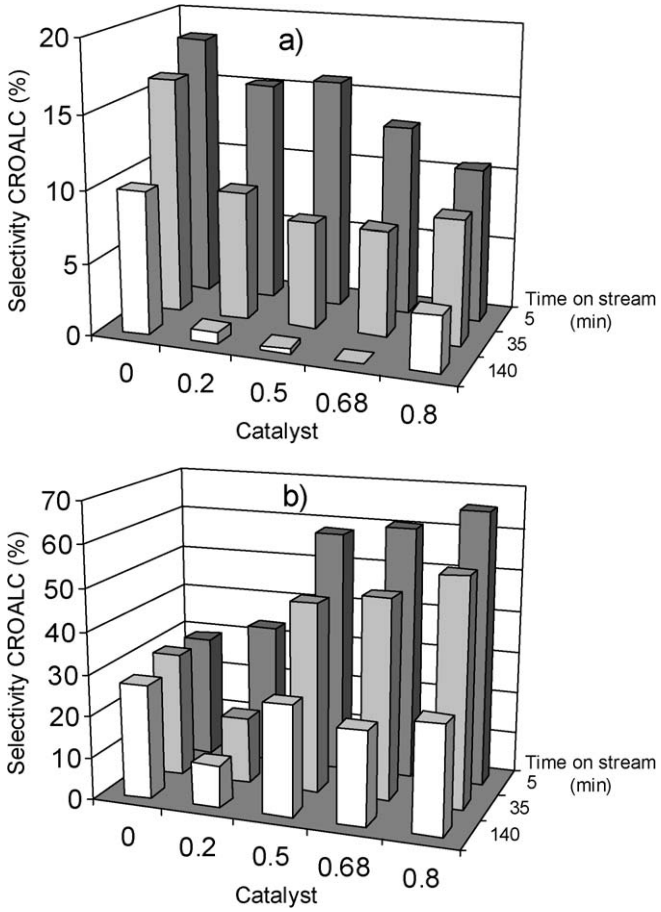

Fig. 13. Selectivity towards crotyl alcohol as a function of time on stream at 333 K for catalysts reduced at (a) 473 K and (b) 773 K.

Table 5
Conversion degrees in crotonaldehyde hydrogenation at different times on stream for catalysts reduced at 473 and 773 K

Catalyst	Reduction at 473 K			Reduction at 773 K		
	5′	35′	140′	5′	35′	140′
Pt/ZrO_2	11.3	3.3	2.6	20.8	6.9	5.0
$Pt/Ce_{0.20}Zr_{0.8}O_2$	6.0	2.1	1.5	7.3	3.2	2.5
$Pt/Ce_{0.5}Zr_{0.5}O_2$	8.9	2.6	2.0	20.1	5.8	3.6
$Pt/Ce_{0.68}Zr_{0.32}O_2$	9.4	2.9	1.9	14.0	3.4	2.1
$Pt/Ce_{0.8}Zr_{0.2}O_2$	14.7	3.4	2.5	17.3	3.4	1.9

These data can be explained in terms of the metal–support interaction, which produces the formation of new sites in the metal–support interface. These new sites created under thermal treatment (reduction at 773 K) constitute coordinative unsaturated Ce^{3+} cations (ceria with oxygen vacancies, CeO_{2-x}) on the support. The interaction of the oxygen atom of the carbonyl group in crotonaldehyde with the Ce^{3+} cations can activate it, thereby favoring its hydrogenation by hydrogen atoms adsorbed on the platinum particles or spilled over from the metal to the platinum–support interface. TPR and XPS findings show that cerium-rich supports are easier to reduce than those with high zirconium content, and although the relative amount of Ce^{3+}, as detected by XPS, is similar in all catalysts after reduction at 773 K, its total amount clearly increases with increasing cerium content in the support. Thus, the increased selectivity to crotyl alcohol (hydrogenation of the C=O bond) with increasing cerium in the support that can be reduced seems reasonable, at least while these special sites are active (10–20 min of reaction). Poisoning of these sites by strong adsorption of reactant and/or products would account for the loss of selectivity with time on stream, which is also accompanied by a decrease in overall activity.

For the cerium-free catalyst Pt/ZrO_2, an enhancement of selectivity toward crotyl alcohol after high-temperature reduction is also observed. TPR measurements show that the ZrO_2 support is not reduced. Further, the TPR profile of Pt/ZrO_2 shows no reduction peak. However, XPS data indicate that at high reduction temperatures, the Pt/Zr atomic ratio decreases. In addition, a slight decrease in the activity value for toluene hydrogenation after reduction at 773 K could indicate a lower number of accessible platinum sites at these conditions. Coq et al. [58], in a study of zirconia-supported ruthenium catalysts in cinnamaldehyde hydrogenation, proposed the formation of specific sites, $Ru–ZrO_x$, at the periphery of the Ru particles, for the catalyst reduced at 623 K, to explain the enhanced selectivity toward cinnamyl alcohol. TPR measurements were done to evaluate this proposition. In addition, the presence of reduced zirconia (Zr^{3+}) in the Au/ZrO_2 system has been detected by ESR [66]. For Pt/ZrO_2, it has been reported that hydrogen spillover occurs at reduction temperatures above 823 K [59]. In our case, the formation of $Pt–ZrO_x$ sites at the metal–support interface seems unlikely, because reduction was carried out at only 773 K and TPR results indicated no appreciable reduction peaks. Furthermore, the Zr $3d_{5/2}$ level binding energy showed no shift with increasing reduction temperature, remaining stable at 182.2 eV (which is the typical binding energy for Zr in ZrO_2). On the other hand, some authors have reported that Pt can interact with zirconia to form a Pt–Zr alloy phase [60], and even that zirconia can donate electrons to platinum [61], but only after a reduction treatment at elevated temperatures. Another interesting point is that the interaction between Pt and ZrO_2 can induce an epitaxial growth of the metal particles [62]. Thus, platinum particles modify their morphology from a round to a flat shape, characteristic of the low index planes of large particles, which are selective to the formation of unsaturated alcohol [63]. Crotonaldehyde hydrogenation on Pt catalysts has been shown to be structure-sensitive, with selectivity and activity being functions of platinum particle size [57]. Theoretical [64] and single-crystal studies [65] have indicated that the adsorption structures of unsaturated aldehydes depend on the metal surface planes exposed. Beccat et al. showed that Pt(111) exhibits some selectivity to crotyl alcohol, whereas other low-index Pt planes do not [65]. Englisch et al. concluded that increasing the abundance of Pt(111) planes in a catalyst can increase the selectivity to crotyl alcohol [57], which could enhance the catalytic performance (activity and selectivity) of Pt/ZrO_2. But this is not likely to apply in the case of cerium-containing catalysts with $x \geqslant 5$, for which the increase in reduction temperature leads to a decrease in the amount of surface platinum as detected by XPS (Fig. 7). This effect could be assigned to the sintering of platinum particles, growing with a preferential orientation that

could be favorable for the reaction. However, the loss of surface platinum atoms cannot explain the drastic decrease in activity for toluene hydrogenation after reduction at 773 K.

4. Conclusion

Several cerium-zirconium mixed oxides, $Ce_xZr_{1-x}O_2$, with varying compositions were prepared using a co-precipitation method. These mixed oxides were used as supports for platinum catalysts, $Pt/Ce_xZr_{1-x}O_2$. XRD profiles indicate that the support preparation method produces varying cerium-zirconium solid solutions; supports with high cerium content ($x \geqslant 0.5$) have a cubic structure, whereas zirconium-rich supports ($x < 0.5$) have a tetragonal structure. TPR and XPS results conclude that supports with a cubic structure are easier to reduce than those with a tetragonal structure. The metal–support interaction, which is responsible for the decrease in activity for toluene hydrogenation, becomes stronger as cerium content increases. The reduction treatment at high temperature (773 K) partially reduces the support, generating oxygen vacancies and Ce^{3+} cations close to the platinum particles that can electronically modify the catalytic behavior of the noble metal. These sites also can activate the carbonyl bond by interacting with its oxygen atom, thus facilitating its hydrogenation and then increasing selectivity toward the unsaturated alcohol. Selectivity toward crotyl alcohol increases with the amount of cerium in the support, at least until these sites are deactivated.

Acknowledgments

Financial support by the Comisión Interministerial de Ciencia y Tecnología (projects BQU 2000-0467 and BQU 2003-06150) is gratefully acknowledged. J.C. Serrano-Ruiz also thanks the Ministerio de Educación y Ciencia (Spain) for an FPI grant. The authors acknowledge the contributions of Dr. F. Coloma in the XPS measurements and by I. Such in the Raman spectra acquisition.

References

[1] K. Bauer, D. Garbe, Common Fragrance and Flavour Materials, VCH, Weinheim, 1983.
[2] K. Bauer, D. Garbe, Ullman Encyclopaedia, VCH, New York, 1988, A11, p. 141.
[3] K. Weissermel, H.J. Arpe, Industrial Organic Chemistry, Verlag Chemie, Weinheim, 1978.
[4] J. Jeak, J.E. Germain, J. Catal. 65 (1980) 133.
[5] A. Dandekar, M.A. Vannice, J. Catal. 183 (1998) 344.
[6] A. Huidobro, A. Sepúlveda-Escribano, F. Rodríguez-Reinoso, J. Catal. 212 (2002) 94.
[7] M. Cossoni, D. Jokic, D. Murzin, R. Touroude, J. Catal. 188 (1999) 165.
[8] A. Sepúlveda-Escribano, F. Coloma, F. Rodríguez-Reinoso, J. Catal. 178 (1998) 649.
[9] J. Silvestre-Albero, F. Rodríguez-Reinoso, A. Sepúlveda-Escribano, J. Catal. 210 (2002) 127.
[10] M. Abid, G. Ehret, R. Touroude, Appl. Catal. A: Gen. 217 (2001) 219.
[11] B. Bachiller-Baeza, I. Rodríguez-Ramos, A. Guerrero-Ruiz, Appl. Catal. A: Gen. 205 (2001) 227.
[12] A.B. Da Silva, E. Jordao, M.J. Mendes, P. Fouilloux, Appl. Catal. A: Gen. 148 (1997) 253.
[13] J. Barrault, A. Deroault, O. Martin, S. Pronier, Compt. Rend. Acad. Sci.-Ser. IIC-Chem. 2 (1999) 507.
[14] J. Kijenski, P. Winiarek, Appl. Catal. A: Gen. 193 (2000) L1–L4.
[15] R. Malathi, R.P. Viswanath, Appl. Catal. A: Gen. 208 (2001) 323.
[16] P. Reyes, H. Rojas, J.L.G. Fierro, J. Mol. Catal. A: Chem. 203 (2003) 203.
[17] R. Ranga, J. Kaspar, R. Di Monte, S. Meriani, M. Graziani, Catal. Lett. 24 (1994) 107.
[18] C.E. Hori, H. Permana, Y. Simon, A. Brenner, K. More, K. Rahmoeller, D. Belton, Appl. Catal. B: Environ. 16 (1998) 105.
[19] E. Hori, A. Brenner, K. Simon, K. Rahmoeller, D. Belton, Catal. Today 50 (1999) 299.
[20] C. Bozo, F. Gaillard, N. Guilhaume, Appl. Catal. A: Gen. 220 (2001) 69.
[21] J.R. González-Velasco, M. Gutiérrez-Ortiz, J.L. Marc, M.P. González-Marcos, G. Blanchard, Appl. Catal. B: Env. 33 (2001) 303.
[22] K. Chen, Q. Yan, Appl. Catal. A: Gen. 158 (1997) 215.
[23] D. Idriss, H. Hindermann, J.P. Kiennemman, Appl. Catal. 51 (1989) 165.
[24] J.C. Lavalley, J. Saussey, J. Lamotte, R. Breault, J.P. Hindermann, A.J. Kiennemann, J. Phys. Chem. 94 (1990) 5941.
[25] M.L. Turner, P.K. Byers, P.M. Maitlis, Catal. Lett. 26 (1994) 55.
[26] S. Velu, M.P. Kapoor, S. Inagaki, K. Suzuki, Appl. Catal. A: Gen. 245 (2003) 317.
[27] P.D.L. Mercera, J.G. Van Ommen, E.B.M. Dosebrug, A.J. Burggraaf, J.R.H. Ross, Appl. Catal. 71 (1991) 363.
[28] D. Briggs, M.P. Seah, 2nd ed., Practical Surface Analysis, vol. 1, Wiley, 1993.
[29] M. Yashima, H. Arashi, M. Kakihana, M. Yoshimura, J. Am. Ceram. Soc. 77 (1994) 1067.
[30] M.H. Yao, R.J. Baird, F.W. Kunz, T.E. Hoost, J. Catal. 166 (1997) 67.
[31] F. Noroha, E.C. Fendley, R.R. Soares, W.E. Alvarez, D.E. Resasco, Chem. Eng. J. 82 (2001) 21.
[32] M. Alifanti, B. Baps, N. Blangenois, J. Naud, P. Grange, B. Delmom, Chem. Mater. 15 (2003) 395.
[33] G. Colón, M. Pijolat, F. Valdivieso, J. Kaspar, M. Graziani, J. Catal. 168 (1997) 386.
[34] P. Fornasiero, R. Di Monte, G. Ranga-Rao, J. Kaspar, S. Meriani, A. Trovarelli, M. Graziani, J. Catal. 151 (1995) 168.
[35] X.-M. Lin, L.-P. Li, G.-S. Li, W.-H. Su, Mater. Chem. Phys. 69 (2001) 236.
[36] H.C. Yao, Y.F.Y. Yao, J. Catal. 86 (1984) 254.
[37] T. Murota, T. Hasegawa, S. Aozasa, H. Matsui, M. Motoyama, J. Alloys Compd. 193 (1993) 298.
[38] M. Daturi, E. Finocchio, C. Binet, J.-C. Lavalley, F. Fally, V. Pericchon, H. Vidal, N. Hickey, J. Kaspar, J. Phys. Chem. B. 104 (2000) 9186.
[39] A. Trovarelli, F. Zamar, J. Llorca, C. De Leitenburg, G. Dolcetti, J.T. Kiss, J. Catal. 169 (1997) 490.
[40] K. Otsuka, Y. Wang, M. Nakamura, Appl. Catal. A: Gen. 183 (1999) 317.
[41] M. Thammachart, V. Meeyoo, T. Risksomboon, S. Osuwan, Catal. Today 68 (2001) 53.
[42] A. Trovarelli, Catal. Rev.-Sci. Eng. 38 (1996) 439.
[43] P. Burroughs, A. Hammemtt, A.F. Orchard, G. Thornton, J. Chem. Soc. Dalton Trans. (1976) 1686.
[44] A. Laachir, V. Perrichon, A. Badri, J. Lamotte, E. Catherine, J.C. Lavalley, J. El Fallal, L. Hilaire, F. le Normand, E. Quéméré, G.N. Sauvion, O. Touret, J. Chem. Soc. Faraday Trans. 87 (1991) 1601.
[45] A.E. Nelson, K.H. Schulz, Appl. Surf. Sci. 210 (2003) 206.
[46] M.S.P. Francisco, V.R. Mastelaro, P.A.P. Nascente, A.O.A. Florentino, J. Phys. Chem. B. 105 (2001) 10515.
[47] B.M. Reddy, A. Khan, Y. Yamada, T. Kobayashi, S. Loridant, J.-C. Volta, J. Phys. Chem. B. 107 (2003) 11475.
[48] P.W. Park, J.S. Ledford, Langmuir 7 (1996) 1794.
[49] S. Bernal, J.J. Calvino, J.M. Gatica, C.L. Cartes, J.M. Pindado, Catalysis by Ceria and Related Systems, Imp. Coll. Press, 2002, Chapter 4.
[50] S. Bernal, J.J. Calvino, J.M. Gatica, C. Mira, P. Fornasiero, J. Kaspar, Communication to Reunion de la Sociedad Española de Catálisis, 2003.
[51] M. Primet, M. El Azhar, R. Frety, M. Guenin, Appl. Catal. 59 (1990) 153.
[52] E. Rogemond, N. Essayem, R. Frety, V. Perrichon, M. Primet, F. Mathis, J. Catal. 166 (1997) 229.

[53] S.D. Lin, M.A. Vannice, J. Catal. 143 (1993) 554.
[54] P. Meraudeau, J.F. Dutel, M. Dufaux, C. Naccache, Stud. Surf. Sci. Catal. 11 (1982) 95.
[55] S.E. Golunski, H.A. Hatcher, R.R. Rajaram, T.J. Truex, Appl. Catal. B: Env. 5 (1995) 367.
[56] S. Bernal, J.J. Calvino, M.A. Cauqui, J.M. Gatica, C. López Cartes, J.A. Pérez Omil, J.M. Pintado, Catal. Today 77 (2003) 385.
[57] M. Englisch, A. Jentys, J. Lercher, J. Catal. 166 (1997) 25.
[58] B. Coq, P.S. Kunbhar, C. Moureau, P. Moreau, F. Figueras, J. Phys. Chem. 98 (1994) 10180.
[59] D.L. Hoang, H. Berndt, H. Lieske, Catal. Lett. 31 (1995) 165.
[60] R. Szymanski, H. Charcosset, P. Gallezot, P. Massardier, L. Tournayan, J. Catal. 97 (1986) 366.
[61] H. Yoshitake, Y. Iwazawa, J. Phys. Chem. 96 (1992) 1329.
[62] S. Roberts, R. Gorte, J. Phys. Chem. 95 (1991) 5600.
[63] P. Gallezot, A. Giroir-Fendler, D. Richard, Catalysis of Organic Reactions, Dekker, New York, 1991, p. 1.
[64] F. Delbeq, S. Sautet, J. Catal. 152 (1995) 217.
[65] P. Beccat, J.C. Bertolini, Y. Gauthier, J. Massardier, P. Ruiz, J. Catal. 126 (1990) 451.
[66] L. Ilieva, J.W. sobzack, M. Manzoli, B.L. Su, D. Andreeva, Appl. Catal. A: Gen. 291 (2005) 85.